

Mechanism of the 1996–97 non-eruptive volcano-tectonic earthquake swarm at Iliamna Volcano, Alaska

Diana C. Roman · John A. Power

Received: 12 April 2010 / Accepted: 30 November 2010 / Published online: 27 February 2011
© Springer-Verlag 2011

Abstract A significant number of volcano-tectonic (VT) earthquake swarms, some of which are accompanied by ground deformation and/or volcanic gas emissions, do not culminate in an eruption. These swarms are often thought to represent stalled intrusions of magma into the mid- or shallow-level crust. Real-time assessment of the likelihood that a VT swarm will culminate in an eruption is one of the key challenges of volcano monitoring, and retrospective analysis of non-eruptive swarms provides an important framework for future assessments. Here we explore models for a non-eruptive VT earthquake swarm located beneath Iliamna Volcano, Alaska, in May 1996–June 1997 through calculation and inversion of fault-plane solutions for swarm and background periods, and through Coulomb stress modeling of faulting types and hypocenter locations observed during the

swarm. Through a comparison of models of deep and shallow intrusions to swarm observations, we aim to test the hypothesis that the 1996–97 swarm represented a shallow intrusion, or “failed” eruption. Observations of the 1996–97 swarm are found to be consistent with several scenarios including both shallow and deep intrusion, most likely involving a relatively small volume of intruded magma and/or a low degree of magma pressurization corresponding to a relatively low likelihood of eruption.

Keywords Iliamna Volcano · VT earthquake · Earthquake swarms · Stress tensor inversion · Fault-plane solutions

Introduction

Intense swarms of low-magnitude, high-frequency (dominant energy >5 Hz) ‘volcano-tectonic’ (‘VT’) earthquakes are a common occurrence beneath active volcanoes (e.g., Vidale and Shearer 2006). Such swarms are common precursors to volcanic eruptions, and are often one of the earliest detected signals of impending volcanic activity (e.g., Endo et al. 1981; Harlow et al. 1996; Umakoshi et al. 2001). A large number of VT swarms, sometimes accompanied by varying degrees of ground deformation and/or volcanic gas emissions, do not, however, result in an eruption (e.g., Lu et al. 2000; Tanaka et al. 2002; Hirn and Michel 1979). Some of these swarms may represent “failed” eruptions, i.e., instances in which magma has intruded into the shallow crust (generally <2 – 3 km below the surface), even though other processes such as a deep intrusion or an increase in fluid circulation and/or tectonic stress magnitude might in some cases explain the observed seismic unrest equally well (e.g., Vidale and Shearer 2006; Vidale et al. 2006).

Editorial responsibility: S. Moran

This paper constitutes part of a special issue. The complete citation information is as follows

Roman DC and Power JA (2011) Mechanism of the 1996-97 non-eruptive volcano-tectonic earthquake swarm at Iliamna Volcano, Alaska. In: Moran SC, Newhall CG, Roman DC (eds) Failed eruptions: Late-stage cessation of magma ascent. Bull Volcanol 73(2):143–153

Electronic supplementary material The online version of this article (doi:10.1007/s00445-010-0439-7) contains supplementary material, which is available to authorized users.

D. C. Roman (✉)
Department of Geology, University of South Florida,
Tampa, FL 33620, USA
e-mail: droman@cas.usf.edu

J. A. Power
Alaska Volcano Observatory, United States Geological Survey,
4210 University Drive,
Anchorage, AK 99508, USA
e-mail: jpower@usgs.gov

One of the outstanding challenges in volcano monitoring is determining whether or not an episode of unrest will proceed to eruption. Because of complex feedback loops among the various driving and resisting forces that act on a batch of ascending magma, the problem of whether or not a given batch of ascending magma will intersect the Earth's surface may be highly non-linear and only tractable from a probabilistic perspective. Furthermore, it is likely that some episodes of magma ascent may proceed further towards eruption than others (i.e., may rise closer to Earth's surface), defining a continuum of eruption likelihood for episodes of volcanic unrest (e.g., Moran et al. 2010). Thus, a key question in retrospective studies of episodes of unrest that did not lead to eruption is whether the episode represents a "failed" eruption. This question may be addressed from several perspectives, such as analyses of gas ratios (e.g., Burton et al. 2007), surface deformation (e.g., Lu et al. 2000), and the spatial relationship between VT earthquakes and the intruded magma.

In this paper we describe and analyze a non-eruptive VT earthquake swarm that occurred at Iliamna Volcano, Alaska, in 1996–97, with the goal of testing the hypothesis that this swarm represented a "failed" eruption. This episode was closely monitored seismically, visually, and geochemically (gas) by the Alaska Volcano Observatory (AVO), facilitating retrospective analysis of swarm characteristics. Because surface deformation data are not available, we focus on analysis of seismic data to assess probable scenarios for magma intrusion during this episode. Building on an earlier study by Roman et al. (2004a), we first present and analyze an expanded set of double-couple fault-plane solutions (FPS) for the swarm and then use these new data to explore vertical-dike-based models of the driving processes for the swarm and associated unrest. We show that FPS for swarm earthquakes do not appear to be rotated with respect to the regional or background stress field, indicating a small volume of intruded magma. We also show that there is weak evidence to support a model of shallow magma emplacement beneath Iliamna's summit, but that so far, there has been no criterion indicated that would allow a clear distinction whether or not the unrest represents a 'failed' eruption.

Background

Iliamna Volcano is located in the Cook Inlet region of Alaska approximately 250 km southwest of Anchorage, along the highly active northeastern segment of the Aleutian arc (Fig. 1a), and is monitored by AVO. Iliamna has not erupted for ~300 years (Waythomas et al. 2000). Iliamna Volcano has been monitored by a four- (1994–

1996) to six- (1996) station seismic monitoring network consisting mainly of short-period vertical sensors with a natural frequency of 1 Hz (one three-component short-period sensor has operated since 1996). There have been no changes to the Iliamna seismic network since the fall of 1996 (i.e., there were no changes in the seismic network during our study period). Additional details of seismic monitoring at Iliamna Volcano during the study period are given by Jolly et al. (2001) and Roman et al. (2004a).

The 1996–97 swarm (Fig. 1b) began in May 1996 with a burst of 88 earthquakes, recorded over 19 days, with a maximum magnitude of 2.1 (Roman et al. 2004a). A second phase of swarm activity began on August 1 and consisted of almost 3,000 earthquakes with a maximum magnitude of 3.3. Both phases of the swarm occurred over a depth range of -1 to 4 km BSL, and formed a ~7-km-long N-S-elongated cluster centered ~3 km south of Iliamna's summit (Roman et al. 2004a; Statz-Boyer et al. 2009). Using high-precision (~100 m error) relative relocations, Statz-Boyer et al. (2009) demonstrated that the swarm hypocenters propagated southwards as the swarm progressed. We refer to the volume of rock hosting the 1996–97 VT swarm earthquakes as the "swarm volume" from this point forward. Despite elevated seismicity and CO₂/SO₂ emissions, AVO did not change its level of concern color code at any time during the swarm (Neal and McGimsey 1997). Roman et al. (2004a) calculated and inverted double-couple FPS for swarm earthquakes occurring between August 1996 and May 1997, and showed that the distribution of faulting during the swarm was heterogeneous compared to regional faulting. On the basis of this observation and the high levels of CO₂ and SO₂ recorded at Iliamna in 1996–97, they concluded that the swarm was driven by the emplacement of a dike beneath Iliamna and suggested several possible mechanisms for swarm earthquakes, including an increase in the magnitude of tensile stress above a propagating dike (e.g., Ukawa and Tsukahara 1996), a local increase in pore pressure or regional stress magnitude (e.g., Jolly and McNutt 1999), or an increase in the magnitude of compressive stress along the sides of a dike (e.g., Roman et al. 2004b). Earthquake activity beneath Iliamna returned to background levels by June 1997 and there have been no major episodes of unrest at Iliamna since 1996–97.

Expanded observations and models for the 1996–97 episode of unrest

In this study, we present and analyze a total of 52 FPS for the swarm period (including the original 24 presented by

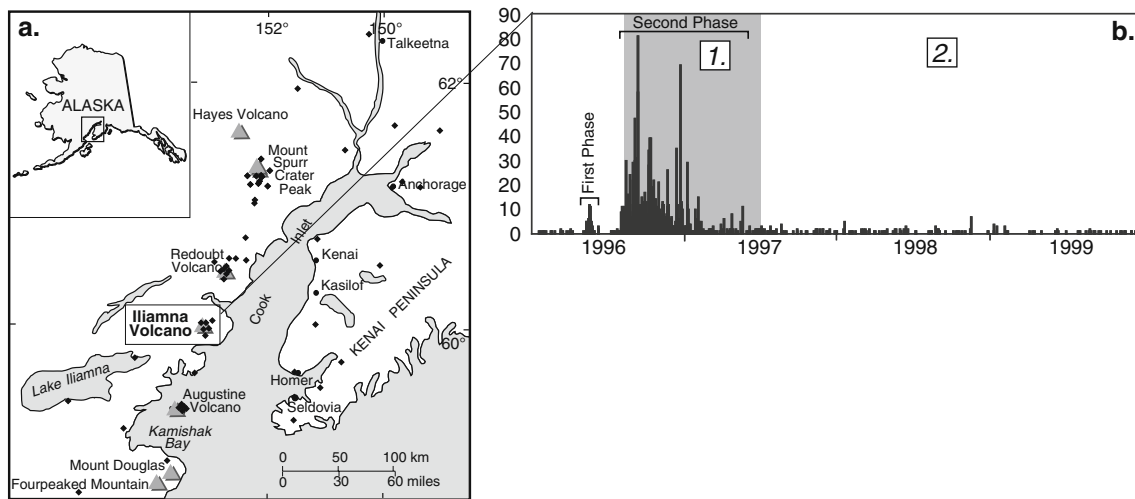


Fig. 1 **a** Map showing the location of Iliamna Volcano (gray triangle) relative to population centers and other volcanoes in the eastern Aleutian arc, and permanent seismic stations in the AVO network (black diamonds). **b** Number of VT earthquakes recorded per day at Iliamna in 1996–1999. Gray box indicates the well-monitored period of swarm activity (following an upgrade to the Iliamna seismic

network), and boxed numbers indicate periods for temporal analyses of stress (delineated by gray/white shading), corresponding to data summarized in Fig. 3. The first (May 1996) and second (August 1996–May 1997) phases of the swarm are indicated with labeled brackets

Roman et al. 2004, which were not reprocessed for this study) and 13 FPS for the background period extending from mid-1997 through 1999. We expand on results presented by Roman et al. (2004a), who included only the shallowest earthquakes in the swarm (−2.5 to 0.8 km BSL), by calculating FPS over a broader depth range of swarm events (−3.0 to 2.5 km BSL). Plots of lower-hemisphere FPS for swarm and background earthquakes are given in Online Resources 1 and 2, respectively. We were only able to calculate FPS for earthquakes occurring from the second phase of the swarm onwards, as only four seismometers were operating on Iliamna prior to August 1996.

All new FPS presented in this study were calculated and analyzed using the same approach and quality criteria of Roman et al. (2004a), which we briefly summarize here. To ensure accuracy and consistency in the FPS data set, earthquakes were first repicked for *P*- and *S*-wave arrival times and *P*-wave first-motion polarities, and relocated using the 1-D velocity model developed for Iliamna by Roman et al. (2004a). FPFIT (Reasenber and Oppenheimer 1985) was then used to calculate FPS for all well-located ($\text{RMS} \leq 0.2$ s, horizontal and vertical location error ≤ 1.5 and azimuthal gap $\leq 180^\circ$) earthquakes with six or more clear first motion polarity picks. Resultant FPS were included in further analysis only if they had a misfit of ≤ 0.15 (15% or less of the polarities inconsistent with the preferred solution), STDR (Station Distribution Ratio, a measure of data distribution with respect to the nodal planes) ≥ 0.4 , an average uncertainty in strike, dip, and rake of $\leq 25^\circ$, and a unique solution or similar multiple solutions. In the case of

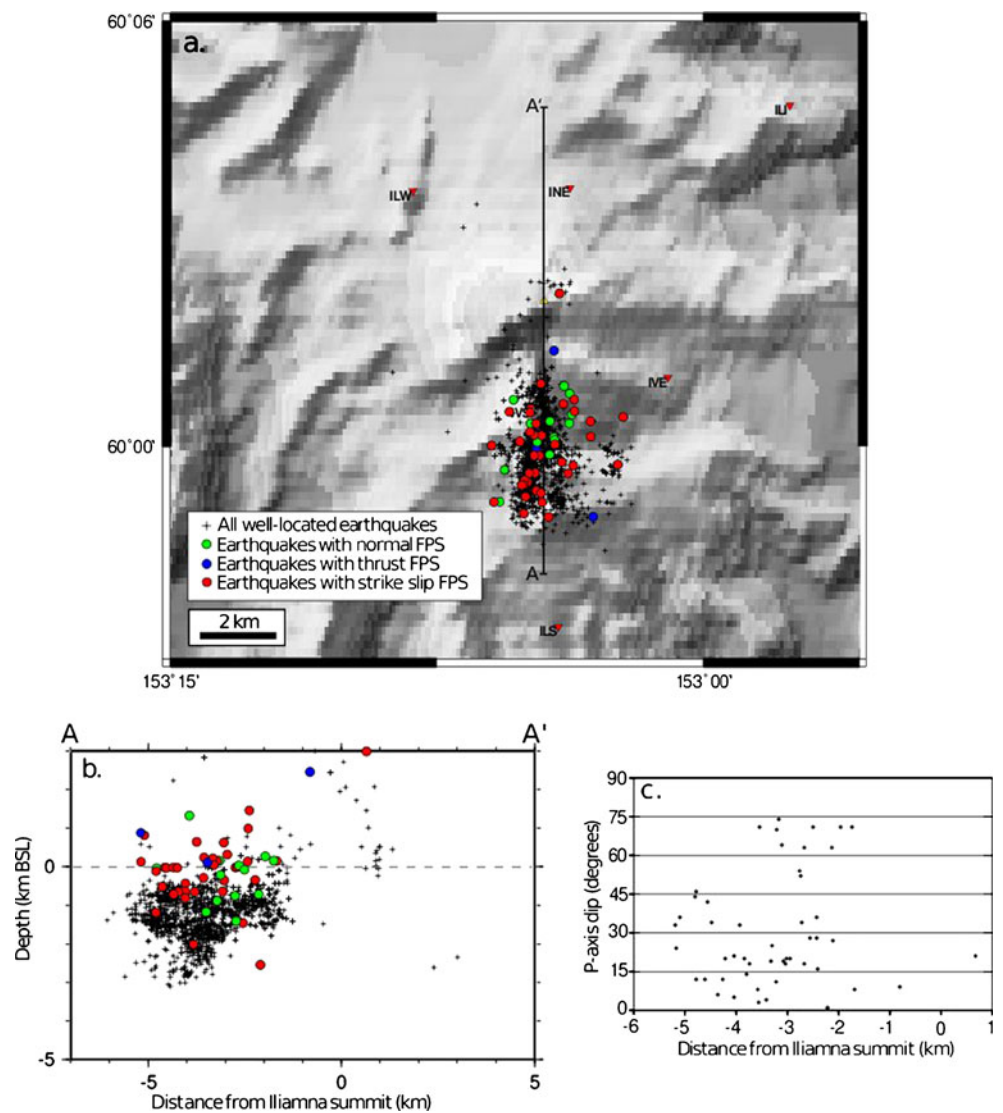
multiple similar solutions, the solution that most exceeded the above criteria was chosen as the preferred solution.

Expanded swarm observations

FPS for swarm earthquakes show primarily a mixture of normal faulting and strike-slip events. We classify FPS as indicating a normal faulting event if the *P*-axis dip is greater than 45° , as strike-slip if both *P*- and *T*-axes have dips less than 45° , and as a thrust or reverse faulting event otherwise. FPS data are summarized by faulting type in map and cross-section views in Fig. 2. Swarm FPS cover the lateral and depth extent of the 1996–97 swarm, and normal faulting events were concentrated in the northern half of the swarm volume, while strike-slip events were distributed throughout the swarm volume. To illustrate this apparent spatial separation between faulting types, we plot *P*-axis dip vs. the distance from Iliamna's summit in Fig. 2c, and identify a cluster of normal faulting events between 1.5 and 3.5 km south of Iliamna's summit.

We next examined fault slip and the orientation of the local stress field during the swarm by inverting all 52 swarm FPS using FMSI ('Focal Mechanism Stress Inversion'; Gephart and Forsyth 1984; Gephart 1990) to obtain an estimate of the stress tensor orientation, following the approach detailed by Roman et al. (2004a). The best-fit stress tensor solution (Fig. 3a) shows a near-vertical σ_1 axis, consistent with the observed normal faulting, but has a relatively high average misfit of 7.26° ,

Fig. 2 **a** Map and **b** N-S cross-section showing the locations of all well-located VT earthquakes recorded at Iliamna Volcano between August 1, 1996–April 30, 1997 (the swarm period). *Black crosses* indicate all well-located earthquakes that do not have well-constrained FPS, *color-coded circles* indicate well-located earthquakes for which well-constrained FPS were obtained. *Green circles* indicate locations of normal-faulting events, *blue circles* indicate locations of thrust/reverse-faulting events, and *red circles* indicate locations of strike-slip events (see text for details). **c** Plot of *P*-axis dip vs. distance from Iliamna's summit. Note the cluster of normal faulting events (*P*-axis dips $>45^\circ$) between 1.5 and 3.5 km south of Iliamna's summit, compared to the broad lateral range of strike-slip faulting events



reflecting local stress field heterogeneity during the swarm consistent with observations of mixed faulting types documented above. Finally, we compared the orientation of swarm strike-slip FPS to the orientation of regional strike-slip faults (documented in Roman et al. 2004a) by plotting a Rose diagram of strike-slip FPS *P*-axes in Fig. 3a. Swarm strike-slip *P*-axes show a clear and consistent NW-SE trend, approximately parallel to the regional orientation of σ_1 and to the direction of plate convergence along the eastern Aleutian arc.

New observations of background seismicity

Although we were only able to calculate 13 well-constrained FPS for a background period of quiescence at Iliamna due to the small magnitudes of background VT earthquakes, these data provide some constraints on the orientation of background stresses in the vicinity of the swarm volume. Following the 1996–97 swarm,

background earthquake activity at Iliamna returned to a small volume directly beneath the summit, but occasional VT earthquakes continued to occur in the swarm volume area (Fig. 4). Of the 13 background FPS presented in this study, six are located in the swarm volume and the remainder locate directly beneath Iliamna's summit. Background FPS consist of a mixture of normal, thrust/reverse, and strike-slip events, but all background normal faulting events are located beneath Iliamna's summit and not within the swarm volume.

The 13 background FPS were inverted to determine the orientation and fit of a best-fit stress tensor (Fig. 3b). The best-fit stress tensor has a NW-oriented subhorizontal σ_1 axis and relatively low misfit of 5.25° , most likely reflecting the small number of background FPS. A Rose diagram of background FPS *P*-axes shows a set of NW- and WNW-oriented trends consistent with the regional stress field and similar to the sense of strike-slip faulting observed during the 1996–97 swarm.

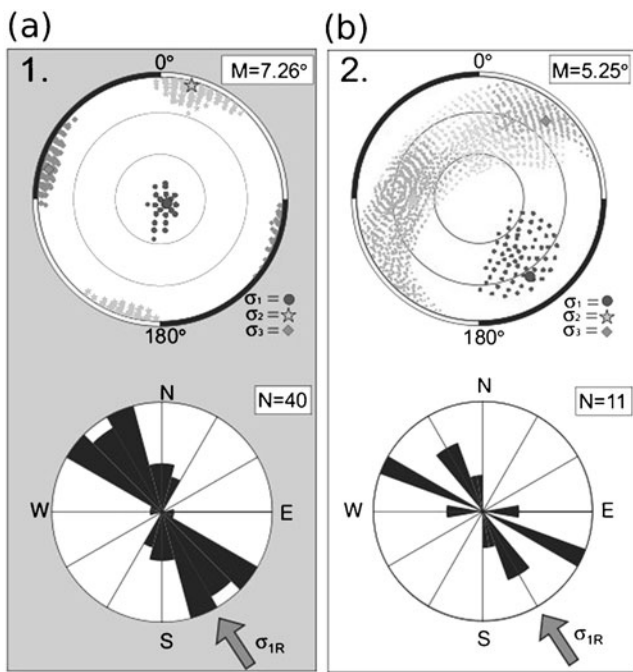


Fig. 3 Rose diagrams of FPS P -axes and best-fit/95% confidence stress tensors for **a** swarm and **b** background VT earthquakes at Iliamna Volcano (time periods correspond to numbered periods in Fig. 1b). Only FPS with P -axis dips greater than 45° are included in Rose diagrams (N indicates the number of FPS shown in each Rose diagram). The left panel includes 24 FPS calculated by Roman et al. (2004a)

Mechanism of the 1996–97 Iliamna non-eruptive swarm

Because of the limited number of FPS and other observational data, including a complete lack of deformation data, there are an infinite number of models that theoretically could be consistent with available data and observations. Our goal in this modeling section is not to obtain a unique model for the mechanism of the 1996–97 swarm, but rather to test four candidate models against all available observations. Specifically, we examine four distinct models that are generally consistent with swarm characteristics (e.g., N-S cluster elongation or southward hypocenter propagation) as detailed below, two of which involve deep magma intrusion, and two of which shallow magma intrusion. In examining these four candidate models, we aim to determine whether it is possible to identify the 1996 swarm as a ‘failed’ eruption; i.e., whether models involving shallow magma emplacement are particularly consistent with swarm observations.

On the basis of significantly elevated CO_2 and SO_2 emissions, and the distinct change in the rate, magnitude, and location of VT earthquakes recorded during the swarm, Roman et al. (2004a) concluded that the swarm resulted from the emplacement of a subvertical dike beneath Iliamna and its southern vents. We now seek to constrain a model for dike emplacement through a combination of stress-field

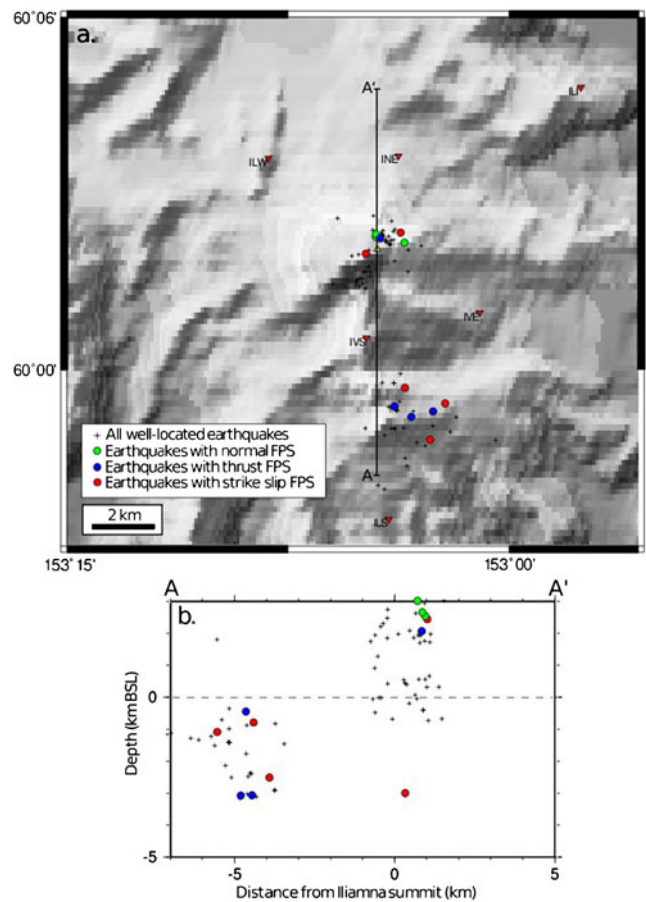


Fig. 4 **a** Map and **b** N-S cross-section showing the locations of all well-located VT earthquakes recorded at Iliamna Volcano between May 1, 1997–December 31, 1999 (the background period). Symbols same as in Fig. 2

modeling and examination of swarm characteristics. In doing so, we focus only on models involving magma emplacement in a vertical dike, as opposed to a vertical cylindrical conduit or a diapir, because the 1996 swarm hypocenters form a vertically- and horizontally-elongate cluster strongly suggestive of a vertical dike (e.g., Fig. 2). Because we are limited in our ability to calculate well-constrained FPS for small-magnitude swarm earthquakes, we also assume that the FPS presented above are representative of all swarm and background earthquakes but note that smaller-magnitude earthquakes could perhaps have had entirely different FPS. Finally, we assume that the swarm earthquakes were triggered directly through a transfer of stress onto faults in the volume of rock surrounding the pressurized magma body (e.g., Rubin and Pollard 1988), rather than indirectly through increased fluid flow in the rock surrounding the magma body as a result of magma degassing or magmatic heating of meteoric fluids (e.g., Jolly and McNutt 1999). The effect of increased fluid flow is to promote fault slip through a reduction of effective normal (“clamping”) stresses on faults (e.g., Scholz

2002). Thus, fluid flow does not modify the local stress field, but simply accelerates the rate of fault slip under existing stress conditions. Because we are interested primarily in examining the link between modeled dike-inflation-induced stresses and observed patterns of fault slip, and not in the absolute magnitude of stresses, exclusion of fluid flow from our analysis does not have a significant impact on the results.

We examine four hypothetical scenarios that are consistent with swarm characteristics and could result in a transfer of stresses consistent with the observed sense and location of faulting during the swarm. The first (“scenario one”) involves intrusion of a shallow NW-SE-trending dike centered beneath the main summit of Iliamna Volcano extending over approximately the same depth range as the swarm volume (Fig. 5). In scenario one, the swarm would hypothetically reflect stresses transmitted laterally by the inflating dike (i.e., the swarm forms one limb of a ‘dogbone’ pattern (e.g., Toda et al. 2002; inset Fig. 5), which is comprised of four limbs extending obliquely from the tips of a dike). This would satisfactorily explain the observed southward propagation of the swarm hypocenters

through time observed by Statz-Boyer et al. (2009) through southward extension of positive Coulomb stresses during gradual dike opening.

The second scenario (“scenario two”) involves intrusion of a deep NW-SE-trending dike centered beneath the 1996–97 swarm, to the south of Iliamna’s summit (Fig. 6). Such an offset between the main vent and center of magma intrusion has been hypothesized elsewhere in the Aleutians, notably at Makushin Volcano (Lu et al. 2002) and Okmok Volcano (e.g., Lu and Dzurisin 2010). In scenario two, the swarm would hypothetically represent a combination of tensile stresses induced above the tip of an inflating dike and ambient (regional) stresses (e.g., Ukawa and Tsukahara 1996). Scenario two is consistent with the observed normal faulting and sense of strike-slip faulting.

The third scenario (“scenario three”) involves a shallow, southward-propagating dike centered 1 km to the south of Iliamna’s summit (Fig. 7), directly beneath a N-S-trending set of Pleistocene-aged satellite vents (Detterman and Hartssock 1966). In scenario three, the swarm would hypothetically represent stresses ahead of the propagating dike tip (e.g., Rubin et al. 1998; Ukawa and Tsukahara 1996). While it is

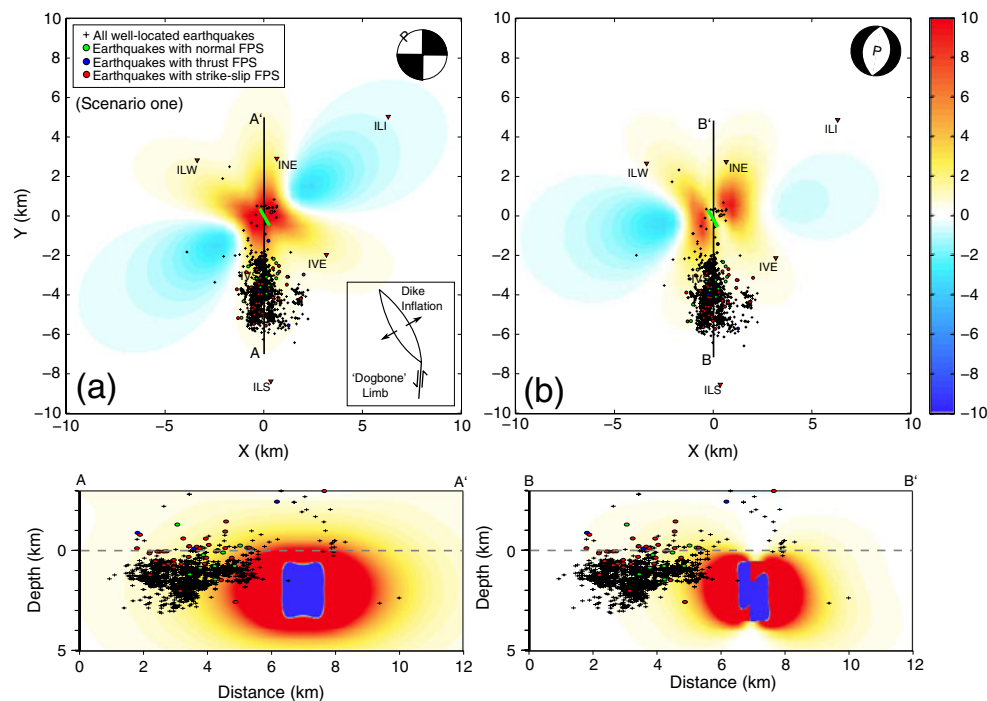


Fig. 5 Map and cross-sections of Coulomb stress changes induced by 1 m inflation of a 1-km-long, N30°W-trending vertical dike centered beneath Iliamna’s summit. Depth extent of the modeled dike is 1–3 km BSL. Map view slice is at 0 km BSL (dashed horizontal line on cross sections). Hot colors (positive Coulomb stress changes) indicate an increased likelihood of earthquake activity (e.g., Toda et al. 2002). Well-constrained locations of Iliamna swarm earthquakes (black dots) are superimposed to allow comparison of modeled regions of increased earthquake likelihood with observed earthquake locations for the modeled sense of slip. **a** Coulomb stress changes on N-S-

striking, vertical left-lateral strike-slip faults (see inset FPS for illustration of receiver fault orientations). Inset diagrams the relationship between the modeled dike and the ‘dogbone’ (Toda et al. 2002) limb of seismicity represented by this scenario. **b** Coulomb stress changes on N10°E-striking, 45°-dipping normal faults (see inset FPS for illustration of receiver fault orientations). Note the strong coincidence of positive zones with observed earthquake locations, and the smaller lateral range of the red zone for normal faulting than for strike-slip faulting (consistent with the observed range of normal faulting vs. strike-slip faulting illustrated in Fig. 2c)

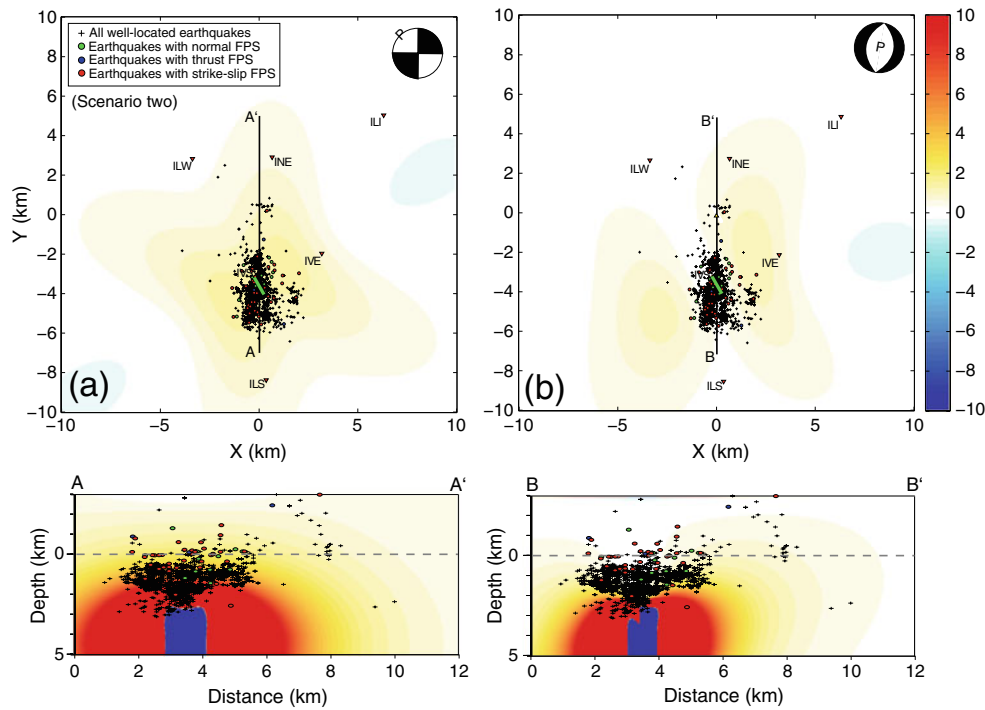
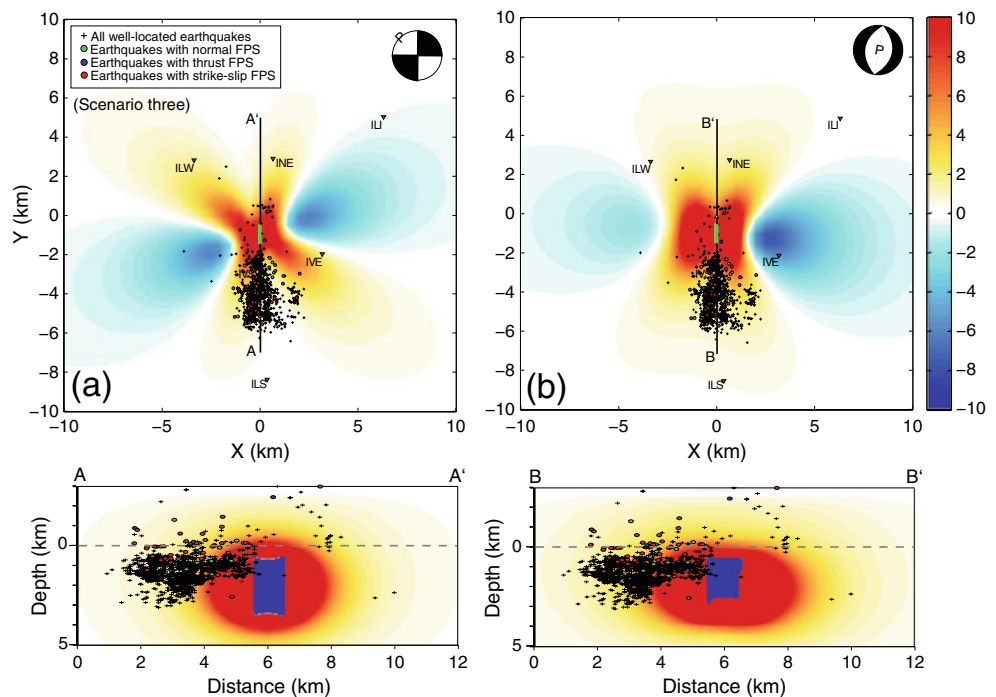


Fig. 6 Map and cross-sections of Coulomb stress changes induced by 1 m inflation of a 1-km-long, N30°W-trending vertical dike centered 3.5 km south of Iliamna’s summit. Depth extent of the modeled dike is 3–6 km BSL. Map view slice is at 0 km BSL (*dashed horizontal lines* on cross sections). Symbols and plotted earthquake locations are the same as in Fig. 5. **a** Coulomb stress changes on N-S-striking, vertical left-lateral strike-slip faults (see inset FPS for illustration of receiver

fault orientations). **b** Coulomb stress changes on N10°E-striking, 45°-dipping normal faults (see inset FPS for illustration of receiver fault orientations). Note again the strong coincidence of positive zones with swarm earthquake locations, and the overlap of the smaller positive zone for normal faulting with the observed range of normal faulting, due to greater proximity of the modeled dike to the region of observed normal faulting (Fig. 2c)

Fig. 7 Map and cross-sections of Coulomb stress changes induced by 1 m inflation of a 1-km-long, N-trending vertical dike centered 1 km south of Iliamna’s summit. Depth extent of the modeled dike is 1–3 km BSL. Map view slice is at 0 km BSL (*dashed horizontal lines* on cross-sections). Symbols and plotted earthquake locations are the same as in Fig. 5. **a** Coulomb stress changes on N-S-striking, vertical left-lateral strike-slip faults (see inset FPS for illustration of receiver fault orientations). **b** Coulomb stress changes on N10°E-striking, 45°-dipping normal faults (see inset FPS for illustration of receiver fault orientations). Note again the strong coincidence of positive zones with swarm earthquake locations for both strike-slip and normal faulting events



also possible in this scenario that the swarm earthquakes represent the propagating dike tip itself, this would require the dike to propagate for ~ 7 km laterally, a less realistic scenario. Scenario three explains the observed southward propagation of the swarm hypocenters through time.

The fourth scenario (“scenario four”) involves a deep NW-SE-trending dike centered beneath Iliamna’s summit (Fig. 8). As in the first scenario, the swarm would hypothetically reflect stresses transmitted laterally and upwards by an inflating dike, potentially explaining the observed normal faulting and southward hypocenter propagation.

We model these four scenarios by mapping Coulomb stress changes produced by dike inflation onto the observed regions of normal and strike-slip faulting during the swarm. By using this approach, we can assess where the modeled stresses are highest and whether modeled regions of positive Coulomb stress coincide with the locations of swarm earthquakes, and whether modeled Coulomb stresses are positive for both normal and strike-slip faulting. We model Coulomb stresses using Coulomb 3.1 (Lin and Stein 2004; Toda et al. 2005), which allows calculation of changes in Coulomb stress caused by an inflating rectangular or point source on faults of specified location, orientation, and sense of slip. All calculations are made in

a homogeneous half-space with standard elastic moduli (shear modulus of 3.2×10^5 MPa, Poisson’s ratio of 0.25, and an effective coefficient of internal friction of 0.4 (e.g., Toda et al. 2005)) and no pore pressure changes or pre-existing stresses. We exclude pre-existing stresses from the models because the orientation and magnitude of the local background stress field at Iliamna is ambiguous and poorly-constrained by FPS data, and an incorrect specification would adversely affect the modeling results. However, we note that in general, pre-existing stress fields with σ_1 and σ_3 parallel and perpendicular to the modeled dikes, respectively, are expected to interfere constructively with the modeled Coulomb stress increases (Roman and Heron 2007). Modeled dikes trend parallel to regional σ_1 (taken as $N30^\circ W$ after Jolly et al. (1994)) in scenarios one, two, and four, and N-S in scenario three (based on the N-S alignment of older volcanic vents at Iliamna, which may reflect a local background stress field characterized by N-S compression). In all scenarios dike inflation is normal to the dike trend and involves 1 m of opening along a 1-km-long, variable-height dike. Finally, we only model ‘static’ inflation, in which dike opening is instantaneous.

The results of Coulomb stress modeling are presented in Figs. 5, 6, 7 and 8. Because of the highly schematic nature

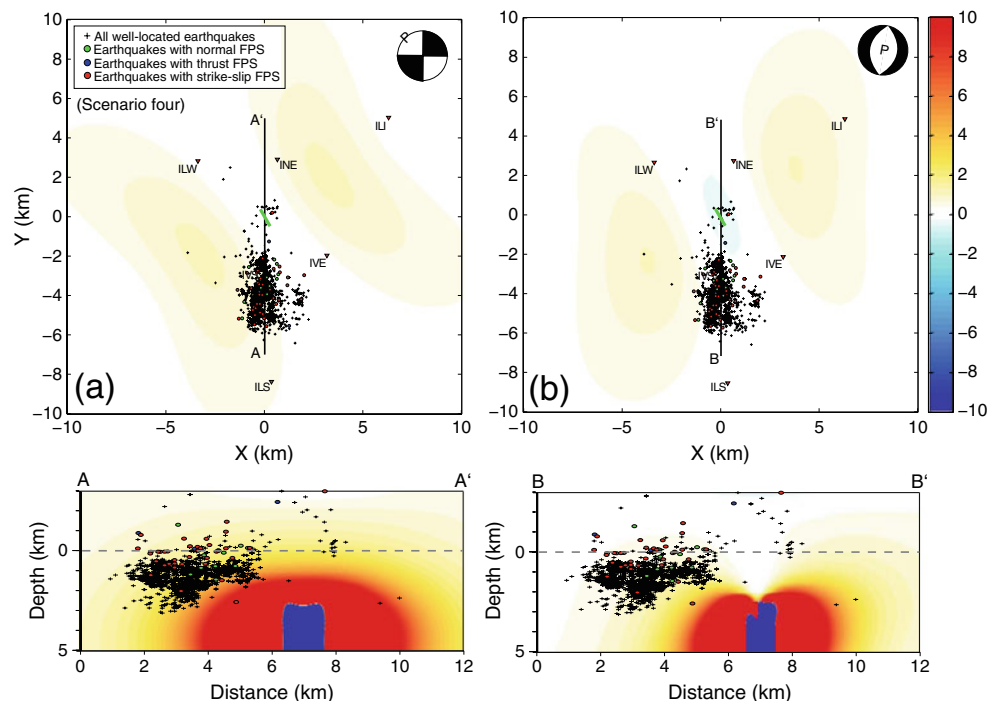


Fig. 8 Map and cross-sections of Coulomb stress changes induced by 1 m inflation of a 1-km-long, $N30^\circ W$ -trending vertical dike centered beneath Iliamna’s summit. Depth extent of the modeled dike is 3–6 km BSL. Map view slice is at 0 km BSL (dashed horizontal line on cross sections). Symbols and plotted earthquake locations are the same as in Fig. 5. **a** Coulomb stress changes on N-S-striking, vertical left-lateral strike-slip faults (see inset FPS for illustration of receiver fault

orientations). **b** Coulomb stress changes on $N10^\circ E$ -striking, 45° -dipping normal faults (see inset FPS for illustration of receiver fault orientations). Note the strong coincidence of positive zones with observed earthquake locations, and the smaller lateral range of the red zone for normal faulting than for strike-slip faulting (consistent with the observed range of normal faulting vs. strike-slip faulting illustrated in Fig. 2c)

of the models we examine, we focus primarily on whether modeled Coulomb stress changes are positive or negative in the regions of observed seismicity (and to a lesser extent on whether the modeled Coulomb stress changes are relatively strong or weak). For scenario one (Fig. 5), zones of positive Coulomb stress change overlap with areas of observed strike-slip and normal faulting during the swarm, indicating that this scenario is consistent with observations of FPS and hypocenter locations. The zone of positive Coulomb stress change for normal faulting does not extend as far south as that for strike-slip faulting, consistent with observed spatial distribution of strike-slip and normal faulting (Fig. 2c). For scenario two (Fig. 6), the zones of positive Coulomb stress change overlap with areas of observed strike-slip and normal faulting during the swarm, indicating that this scenario is also consistent with observations of FPS and hypocenter locations. The zone of positive Coulomb stress change for normal faulting is not as large as that for strike-slip faulting, which is also consistent with tighter clustering of normal faulting events (Fig. 2c) but not as consistent with observed spatial distribution of strike-slip and normal faulting in the swarm volume (Fig. 2c). For scenario three (Fig. 7), the zones of positive Coulomb stress change overlap with areas of observed strike-slip and normal faulting during the swarm, indicating that this scenario is also consistent with observations of FPS and hypocenter locations. For scenario four (Fig. 8), zones of positive Coulomb stress change overlap with areas of observed strike-slip and normal faulting during the swarm, indicating that this scenario, like the other three, is also consistent with observations of FPS and hypocenter locations. The zone of positive Coulomb stress change for normal faulting does not extend as far south as that for strike-slip faulting, which, as in scenario one, is also consistent with observed spatial distribution of strike-slip and normal faulting (Fig. 2c).

Discussion

Based on the results of Coulomb stress modeling and the available observations of the 1996–97 swarm, it is difficult to determine conclusively whether or not magma was emplaced shallowly (i.e., at depths less than 2–3 km), and hence whether the 1996–97 unrest is evidence of a ‘failed’ eruption. All four of the dike-emplacment scenarios we examined were found to be consistent with FPS orientations and the N-S trend formed by swarm earthquakes (regions of modeled Coulomb stress increases all showed approximate N-S trends). In general, Coulomb stress changes within the swarm volume resulting from scenarios for inflation of deep dikes are smaller than in scenarios involving

shallow dike inflation (Figs. 5, 6, 7 and 8), providing support for the two scenarios involving shallow inflation. However, the magnitude of Coulomb stress change is not an ideal proxy for the likelihood of fault slip (e.g., Toda et al. 2002). Knowledge of the background stress field orientation in the swarm volume would allow us to favor either the three scenarios involving a NW-SE-trending dike (consistent with the regional stress field orientation; Roman et al. 2004a), or the single scenario involving a N-S-trending dike (consistent with the N-S alignment of older vents at Iliamna). While *P*-axes of background swarm volume FPS are oriented NW-SE, indicating that NW-SE-trending dikes are favored beneath Iliamna, only six well-constrained background FPS currently characterize the swarm volume (Fig. 3b). Gradual or stepwise opening of a dike (as opposed to the instantaneous opening illustrated by our models) would produce increasingly larger zones of positive Coulomb stress change extending from the model dike through time in all cases, potentially accounting for the observed southward propagation of hypocenters during the 1996–97 swarm (Statz-Boyer et al. 2009).

In sum, we find only weak evidence to favor a model of shallow magma intrusion. While a model of scenario one, involving gradual inflation of a shallow, NW-oriented dike beneath Iliamna’s summit, produces relatively strong Coulomb stress increases in the swarm volume and is consistent with the orientation of the regional stress field and background swarm volume FPS *P*-axes, the off-summit location and N-S trend in swarm hypocenters, the southward migration of swarm seismicity, and measurements of strong SO₂ and CO₂ emissions above Iliamna’s summit, we cannot rule out models involving off-vent deep magma intrusion or shallow lateral magma migration.

Regardless of its depth, the swarm FPS suggest that the intrusion was relatively small in volume. We speculate that the intrusion may have stalled for this reason (e.g., Taisne et al. 2010). In particular, swarm FPS do not appear to reflect stresses produced in the walls of a shallow dike, which are sometimes observed as FPS with *P*-axes oriented ~90° to regional maximum compression (e.g., Roman et al. 2004b; Lehto et al. 2010; Umakoshi et al. 2001). A possible explanation for the inferred absence of VT earthquakes along the dike walls is that stresses induced by dike inflation were low in magnitude, due to the small volume and/or low overpressure of the intruded magma. The local stress field induced by dike inflation is spatially variable, consisting of two zones extending from the walls of the dike in which inflation-induced stresses are perpendicular to regional (ambient) stresses and four zones extending obliquely from the dike tips in which inflation-induced stresses are parallel to regional stresses

(e.g., Rubin and Pollard 1988). Dike-inflation-induced stresses which are parallel to regional stresses combine constructively with the regional stress field to induce failure in the zones extending obliquely from the dike tips. In the dike walls, however, induced stresses must be strong enough to overcome regional stresses to produce earthquakes with a reversed sense of slip (i.e., a $\sim 90^\circ$ rotation of FPS *P*-axes). Thus, low-magnitude inflation-induced stresses (corresponding to low magma volumes and/or low overpressure) are more likely to result in VT earthquakes with FPS consistent with regional stresses in zones extending from the dike tips, as observed at Iliamna in 1996–97.

Ultimately, a comprehensive framework is necessary for the interpretation of VT seismic swarms in terms of eruption likelihood. Such assessments are complicated by the fact that swarms can be influenced by different amounts of emplaced magma or levels of magma pressurization, different regional stress magnitudes and/or orientations or host rock strength conditions, and/or different magma rheologies, all of which may combine in different ways to produce similar swarm characteristics. For this reason, analysis of seismic data alone may not be sufficient to determine the cause of an episode of unrest, and combined analysis of seismic, gas and surface deformation data may in many cases be critical for distinguishing among different models for the observed unrest. Furthermore, it is critical to interpret a given episode of unrest independently as well as in comparison to other well-documented swarms. Worldwide, however, only a small number of VT earthquake swarms associated with ‘failed’ eruptions have been well-studied (e.g., analysis of relative earthquake locations and/or fault-plane solutions). In this study, we have shown that several dike-intrusion scenarios are consistent with characteristics of the VT earthquake swarm at Iliamna in 1996–97. We have also shown that careful analysis of VT earthquake swarm mechanisms in conjunction with other volcanological observations may help constrain the role of magma in driving an episode of volcanic unrest, but that it may be difficult in many cases to confidently identify an episode of magma intrusion as a ‘failed’ eruption.

Acknowledgements We are extremely grateful for thorough and constructive reviews from Zhong Lu, Matt Haney, Jackie Caplan-Auerbach, Seth Moran, and an anonymous reviewer. DCR also thanks Chris Newhall and Paul Segall for illuminating discussions of possible mechanisms for the Iliamna earthquake swarm.

References

- Burton M, Allard P, Muré F, La Spina A (2007) Magmatic gas composition reveals the source depth of slug-driven Strombolian explosive activity. *Science* 317:227–230
- Detterman RL, Hartsock JK (1966) Geology of the Iniskin-Tuxedni Region, Alaska. US Geol Surv Prof Pap 512:1–76
- Endo ET, Malone SD, Noson LL, Weaver CS (1981) Locations, magnitudes, and statistics of the March 20–May 18 earthquake sequence. In: Lipman PW, Mullineaux DR (eds) The 1980 Eruptions of Mount. St. Helens, Washington. US Geol Surv Prof Pap 1250:93–107
- Gephart JW (1990) FMSI—a fortran program for inverting fault slickenside and earthquake focal mechanism data to obtain the regional stress-tensor. *Comput Geosci* 16:953–989
- Gephart JW, Forsyth DW (1984) An improved method for determining the regional stress tensor using earthquake focal mechanism data: application to the San Fernando earthquake sequence. *J Geophys Res* 89:9305–9320
- Harlow DH, Power JA, Laguerta EP, Ambubuyog G, White RA, Hoblitt RP (1996) Precursory seismicity and forecasting of the June 15, 1991, eruption of Mount Pinatubo. In: Newhall CG, Punongbayan RS (eds) Fire and mud: Eruptions and Lahars of Mount Pinatubo, Philippines. Univ Washington Press, Seattle, pp 285–306
- Hirn A, Michel B (1979) Evidence of migration of main shocks during major seismo-volcanic crises of La Soufrière (Guadeloupe, Lesser Antilles) in 1976. *J Volcanol Geotherm Res* 6:295–304
- Jolly AD, McNutt SR (1999) Seismicity at the volcanoes of Katmai National Park, Alaska: July 1995–December 1997. *J Volcanol Geotherm Res* 93:173–190
- Jolly AD, Page RA, Power JA (1994) Seismicity and stress in the vicinity of Mount Spurr volcano, south central Alaska. *J Geophys Res* 99:15305–15318
- Jolly AD, Stihler SD, Power JA, Lahr JC, Paskievitch J, Tytgat G, Estes S, Lockhart AB, Moran SC, McNutt SR, Hammond WR (2001) Catalog of earthquake hypocenters at Alaskan Volcanoes: January 1994 through December 31, 1999. US Geol Surv Open-File Rep 01–189
- Lehto HL, Roman DC, Moran SC (2010) Temporal changes in stress preceding the 2004–2008 eruption of Mount St. Helens, Washington. *J Volcanol Geotherm Res* 198:129–142
- Lin J, Stein RS (2004) Stress triggering in thrust and subduction earthquakes and stress interaction between the southern San Andreas and nearby thrust and strike-slip faults. *J Geophys Res* 109:B02303. doi:10.1029/2003JB002607
- Lu Z, Dzurisin D (2010) Ground surface deformation patterns, magma supply, and magma storage at Okmok volcano, Alaska, from InSAR analysis: 2. Coeruptive deflation, July–August 2008. *J Geophys Res* 115:B00B03. doi:10.1029/2009JB006970
- Lu Z, Wicks C, Power JA, Dzurisin D (2000) Ground deformation associated with the March 1996 earthquake swarm at Akutan volcano, Alaska, revealed by satellite radar interferometry. *J Geophys Res* 105:21483–21495
- Lu Z, Power JA, McConnell VS, Wicks C, Dzurisin D (2002) Preeruptive inflation and surface interferometric coherence characteristics by satellite radar interferometry at Makushin volcano, Alaska: 1993–2000. *J Geophys Res* 107:2266. doi:10.1029/2001JB000970
- Moran SC, Newhall C, Roman DC (2010) Failed eruptions: when restlessness leads to quiescence. *Bull Volcanol*: this volume
- Neal CA, McGimsey RG (1997) Volcanic activity in Alaska and Kamchatka: summary of events and response of the Alaska Volcano Observatory. US Geol Surv Open-File Rep 97–433
- Reasenber P, Oppenheimer DH (1985) FPFIT, FPLOT and FPPAGE; Fortran computer programs for calculating and displaying earthquake fault-plane solutions. US Geol Surv Open-File Rep 85–739
- Roman DC, Heron P (2007) Effect of regional tectonic setting on local fault response to episodes of volcanic activity. *Geophys Res Lett* 34:L 13310. doi:10.1029/2007GL030222

- Roman DC, Power JA, Moran SC, Cashman KV, Doukas MP, Neal CA, Gerlach TM (2004a) Evidence for dike emplacement beneath Iliamna Volcano, Alaska in 1996. *J Volcanol Geotherm Res* 130:265–284
- Roman DC, Moran SC, Power JA, Cashman KV (2004b) Temporal and spatial variation of local stress fields before and after the 1992 eruptions of Crater Peak Vent, Mount Spurr Volcano, Alaska. *Bull Seismol Soc Am* 94:2366–2379
- Rubin AM, Pollard DD (1988) Dike-induced faulting in rift zones of Iceland and Afar. *Geology* 16:413–417
- Rubin AM, Gillard D, Got J-L (1998) A reinterpretation of seismicity associated with the 1983 dike intrusion at Kilauea Volcano, Hawaii. *J Geophys Res* 103:10003–10015
- Scholz CH (2002) *The mechanics of earthquakes and faulting*, 2nd edn. Cambridge University Press, Cambridge
- Statz-Boyer P, Thurber C, Pesicek J, Prejean S (2009) High-precision relocation of earthquakes at Iliamna Volcano, Alaska. *J Volcanol Geotherm Res* 184:323–332
- Taisne B, Tait S, Jaupart C (2010) Conditions for the arrest of a vertical propagating dyke. *Bull Volcanol*: this volume
- Tanaka S, Hamaguchi H, Ueki S, Sato M, Nakamichi H (2002) Migration of seismic activity during the 1998 volcanic unrest at Iwate volcano, northeastern Japan, with reference to P and S wave velocity anomaly and crustal deformation. *J Volcanol Geotherm Res* 113:399–414
- Toda S, Stein RS, Sagiya T (2002) Evidence from the AD 2000 Izu islands earthquake swarm that stressing rate governs seismicity. *Nature* 419:58–61
- Toda S, Stein RS, Richards-Dinger K, Bozkurt S (2005) Forecasting the evolution of seismicity in southern California: animations built on earthquake stress transfer. *J Geophys Res* 110:B05S16. doi:10.1029/2004JB003415
- Ukawa M, Tsukahara H (1996) Earthquake swarms and dike intrusions off the east coast of Izu Peninsula, central Japan. *Tectonophysics* 253:285–303
- Umakoshi K, Shimizu H, Matsuwo N (2001) Volcano-tectonic seismicity at Unzen Volcano, Japan, 1985–1999. *J Volcanol Geotherm Res* 112:117–131
- Vidale JE, Shearer PM (2006) A survey of 71 earthquake bursts across southern California: exploring the role of pore fluid pressure fluctuations and aseismic slip as drivers. *J Geophys Res* 111: B05312. doi:10.1029/2005JB004034
- Vidale JE, Boyle KL, Shearer PM (2006) Crustal earthquake bursts in California and Japan: their patterns and relation to volcanoes. *Geophys Res Lett* 33:L20313. doi:10.1029/2006GL027723
- Waythomas CF, Miller TP, Beget JE (2000) Record of Late Holocene debris avalanches and lahars at Iliamna Volcano, Alaska. *J Volcanol Geotherm Res* 104:97–130